Quantitative Analysis of Modulations in Numerical and Lateral Distribution of Intramembrane Particles during the Cell Cycle of Neuroblastoma Cells

S. W. DE LAAT, L. G. J. TERTOOLEN, P. T. VAN DER SAAG, J. G. BLUEMINK
Hubrecht Laboratory, International Embryological Institute, 3584 CT Utrecht, The Netherlands

ABSTRACT Modulations in the internal structure of the plasma membrane during the cell cycle of mouse C1300 neuroblastoma cells (clone Neuro-2A) have been studied by freeze-fracture electron microscopy. Both the numerical and lateral distributions of the intramembrane particles (IMP) of the P face of the medium-exposed plasma membrane were determined as a function of the IMP diameter. The lateral IMP-distribution was quantitified by a differential density distribution analysis, that could distinguish between random, aggregated, and dispersed distributions of IMP-subpopulations at various levels of spatial organization. Nonrandom lateral IMP-distribution was considered to indicate significant directional constraints on the lateral mobility of the represented molecules. The analysis demonstrated that the density, the size distribution, and the lateral distribution of the IMP are modulated during the cell cycle, such that characteristic structural and dynamic membrane properties can be attributed to the various cell cycle phases (M, G_1, S, and G_2). The results are interpreted in terms of asynchronous assembly of different membrane components and dynamic reorganizations within the plasma membrane during the cell cycle. Furthermore, they provide a structural manifestation of earlier observed changes in the dynamic properties of membrane proteins and lipids, and functional membrane transport properties in these neuroblastoma cells.

Cell-cycle-dependent modulations have been described for a variety of plasma membrane properties, such as membrane composition, receptor expression, electrical properties, transport processes, activity of membrane-bound enzymes, suface architecture, etc. (for reviews, see references 1, 11, 12, 18, 19). Such studies have implied that the plasma membrane is a key organelle for growth regulation. Little is known about possible ultrastructural modifications of the plasma membrane through the cell cycle that might reflect intrinsic membrane changes. Such information can be obtained by freeze-fracture electron microscopy, which provides a high resolution visualization of the internal structure of biological membranes (6). The intramembrane particles (IMP) visualized in the fracture plane through the membrane lipid matrix most likely represent integral membrane (glyco) proteins (23).

In previous studies we have shown that neuroblastoma cells (clone Neuro-2A) are a suitable system for cell cycle studies. These cells can be synchronized by selective detachment of mitotic cells and have a relatively short division cycle of ~10 h (14, 26). Cell-cycle-dependent modulations in membrane lipid fluidity (14), lateral mobility of membrane lipids and proteins (13), electrical membrane properties, and passive and active cation transport properties (4, 16, 17) have been described by us for these cells. Furthermore, some of these membrane alterations, e.g. in Na^+-transport and (Na^+-K^+)ATPase activity, were shown to be necessary for a normal progression through particular phases of the cell cycle (16, 17). The investigated membrane properties change largely in parallel during the cell cycle such that unique physicochemical states of the plasma membrane can be attributed to the various cell cycle phases. This suggests that common intrinsic membrane modulations are underlying the observed alterations, possibly originating from asynchronous assembly of different membrane components (11, 12). Support for this view comes from a number of studies on the synthesis and incorporation of a variety of membrane components in various cells (for references, see [1]).

An ultrastructural analysis by freeze-fracture electron microscopy could provide direct and quantitative information on the intrinsic membrane modulations during the cell cycle. So far, only a few studies on this subject have been published, all restricted to an analysis of the total IMP density, and giving

THE JOURNAL OF CELL BIOLOGY · VOLUME 96 APRIL 1983 1047-1055

contradictory results (10, 21, 25). Furthermore, correlations between observed structural changes and membrane functions have not yet been made.

Recently, we developed an improved method to describe freeze-fracture images quantitatively in terms of: (*a*) the numerical IMP-density; and (*b*) the lateral IMP-distribution; both as a function of the IMP diameter (15). Determination of the total IMP-density and IMP-size distribution may indicate the preferential insertion of (specific) lipids or proteins, the vertical displacement of the represented molecules or alterations in the fracture plane of the membrane, and the aggregation and dissociation of macromolecules within the membrane. The analysis of the lateral IMP-distribution provides a means to interpret static freeze-fracture images in terms of the dynamic behavior of membrane components. In the absence of significant directional constraints on the lateral mobility of the molecules represented by the IMP, the IMP will acquire at any given time a random distribution in the plane of the membrane. Directional forces acting upon these molecules will lead to a nonrandom IMP distribution, whereby aggregative and dispersive (more uniform than random) distributions might be distinguished (15). In the present study we have applied this method to analyze the changes in the internal structure of the plasma membrane during the cell cycle of Neuro-2A cells.

MATERIALS AND METHODS

Cell Culture and Synchronization: C1300 mouse neuroblastoma cells, clone Neuro-2A, were grown in Dulbecco's modified Eagle's medium, without bicarbonate, containing 25 mM N-2-hydroxy ethylpiperazine N'-2 ethanolsulfonic acid (HEPES) buffer (pH 7.5) and 10% fetal calf serum. Synchronized cell populations were obtained by selective detachment of mitotic cells upon shaking of the culture flasks, as described (14), and subsequent replating on glass coverslips at 2–3 × 10^4 cells/cm^2. At this cell density, cell contacts are nearly absent. Routinely, the degree of synchrony and the progression through the cell cycle were determined by [^{3}H]thymidine incorporation and time-lapse cinematography, as described (14). In these experiments the mean cell doubling time was 11 h, subdivided in M, G_1, S, and G_2 phases of 0.5, 3.5, 5, and 2 h, respectively.

Preparation of Cells: At different times after mitosis, synchronized cells on glass coverslips were washed in PBS and fixed for 10 min at 37°C in prewarmed 2.5% glutaraldehyde in PBS pH 7.4. After fixation, the samples were washed three times in PBS, incubated for 10 min in 20% glycerol in PBS, rapidly frozen in a mixture of solid and liquid nitrogen, and fractured by a double replica technique, as described before (2). For freeze-fracture of mitotic cells, cells were washed in PBS immediately after shake-off and also fixed for 10 min in 2.5% glutaraldehyde in PBS. After fixation, a cell pellet was obtained by gentle centrifugation and was placed in a specimen holder and fractured, as described before (3). In all cases a homogeneous ice structure without detectable crystal formation was observed, indicating proper sample freezing.

Analysis of Electron Micrographs: Details of the analysis of the electron micrographs and of the applied statistical methods have been described elsewhere (15). Conditions for reproducible electron microscopic recording were those described before (2). Electron micrographs were selected upon the following criteria: (*a*) The replica should be perpendicular to the optical axis of the electron microscope; (*b*) the replica should show a sufficient resolution to discriminate IMP at a 10 Å resolution. Surface irregularities, such as microvilli, were not taken into account. Electron micrographs of replicas of 0.5 μm^2 plasma membrane areas of the perikaryon region of the medium-exposed side of the cell were analyzed at a final magnification of 252,000, using a digitizer table with writing digitizer stylus on-line connected to a Wang 2200 microcomputer. This system allowed for a reproducible spatial resolution of 10 Å. The diameter and relative position of each IMP in the micrograph were determined by digitizing the coordinates of both sides of the widest part of the particle shadow, perpendicular to the shadowing direction. The distance between each pair of coordinates was used as a measure for the IMP diameter; the relative positions of the IMP in the plane of the replica were used for the analysis of the lateral IMP-distribution. It will be clear that subjective criteria are being used here to discriminate between IMP and other inhomogeneities in the replica. For P-faces the difference in the number of IMP and their diameter distribution, thus determined by different persons, were <5%. In E-faces, however, IMP are less distinct and these differences could amount to up to 25%. For that reason, an analysis of E-faces can give only limited information, and quantitative data regarding the E-face should be considered with some caution.

We have analyzed, in general, 10 electron micrographs of P- as well as E-faces, each representing 0.5 μm^2 membrane area of different cells, for each of 14 time points in the cell cycle. All cells were obtained by a single mitotic selection procedure. A detailed quantitative analysis will be given only for P-faces, in which a total number of 72,462 IMP was digitized. In view of the reproducibility problem, mentioned above, we will include data on the E-face only so far as they can contribute to a qualitative interpretation of the observed changes in membrane structure.

Numerical IMP-Distribution: The measured IMP-diameters were subdivided into classes of 10 Å difference, and frequency distributions of IMP-diameter classes were obtained by counting the number of scored IMP per class. Taking into account the membrane area represented by the micrograph, we could calculate the IMP-density.

Lateral IMP-Distribution: The digitized coordinates of the relative positions of the individual IMP on the electron micrograph and their calculated diameters provide the data for analyzing the lateral or two-dimensional distribution of IMP of a selectable diameter range. The characterization of the lateral IMP-distribution is based on a differential IMP-density distribution analysis, in detail described before (15).

To this end an electron micrograph, representing a membrane area of 0.5 μm^2, is subdivided into square subareas with a selectable grid size, and the number of IMP per subarea is counted. The frequency distribution of the number of subareas as a function of the number of IMP per subarea is then statistically compared with a hypothetical random IMP-distribution. For a random distribution, this frequency distribution would follow a Poisson distribution (24), characterized by the fact that its mean equals its variance. The probability of a random distribution is obtained by calculating the approximate normal deviate (Z) in a Poisson variance test (24). For a theoretical random or Poisson distribution Z = O, positive and negative Z-values indicate aggregative and dispersive tendencies, respectively. Absolute Z-values of 1.65, 2.33, and 3.10 give 5%, 1%, and 0.1% significance levels, respectively.

A 1% significance level is used to discriminate between random and nonrandom lateral IMP-distribution. It should be realized that Z is independent from the number of subareas chosen for the subdivision of the electron micrograph, thereby being a suitable statistical measure for possible deviations from randomness. Two parameters can be varied in the analysis: (*a*) the diameter range of the IMP to be involved in the analysis, whereby the lateral distribution can be characterized for IMP subclasses, and (*b*) the grid size used for subdividing the membrane area. This latter feature appears to be an extremely useful one. It allows us to distinguish heterogeneities within the IMP-density distribution at different spatial resolution. A given IMP pattern might show up to be random at a certain grid size, and either dispersive or aggregative at another. In practice, we have analyzed all distributions at grid sizes of three times and six times the maximum diameter of the selected IMP, respectively. Increasing the grid size further did not yield significant new information.

RESULTS

Total IMP-Density

Visual inspection of replicas of P-faces prepared from cells at different time points in the cell cycle (Fig. 1) reveals evident differences in the IMP density. As a first step in the analysis, the total IMP density, expressed as the number of IMP/μm^2, was determined at different time points. Usually, 10 electron micrographs, each representing 0.5 μm^2, were analyzed for each time point. Fig. 2 shows that the total IMP density decreases sharply during the early G_1-phase from 1,254 IMP/μm^2 at mitosis to 690 IMP/μm^2 1 h after mitosis, which is a minimum during the cell cycle. This decrease is followed by a gradual increase during the remaining part of the G_1-phase to 1,130 IMP/μm^2 at 4 h after mitosis. Early S-phase is characterized by a more rapid increase, resulting finally in a maximal IMP-density of 1,685 IMP/μm^2 by the end of S-phase (8 h). Before cells re-enter mitosis, the IMP density decreases again.

In particular, mitotic cells show large variations in IMP density within a single cell. These cells show a relatively large number of surface irregularities, which are partially or completely devoid of IMP (not shown). As we took necessarily only plane membrane areas into account, the given IMP density is certainly an overestimate. However, even in these areas the

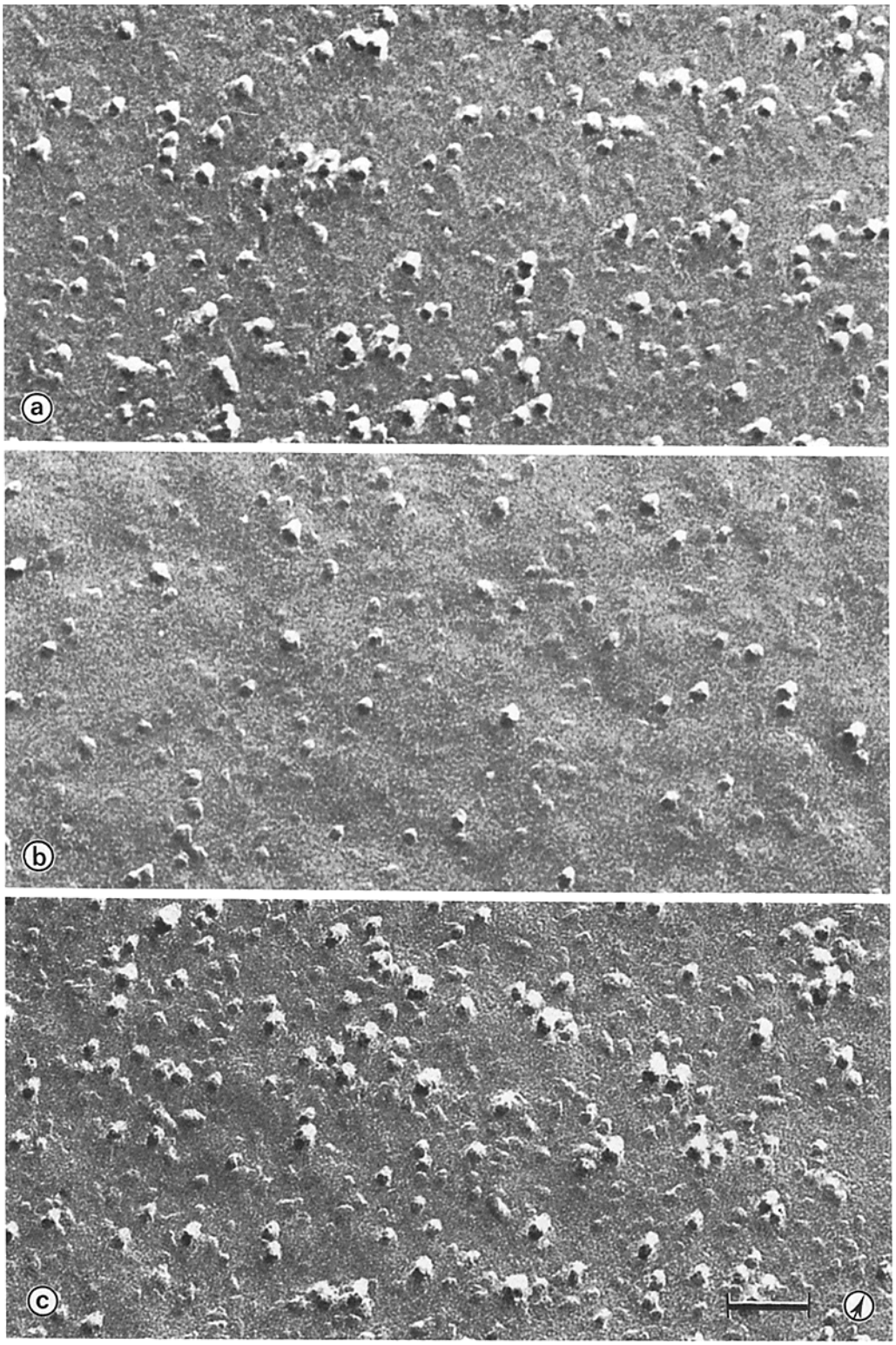

FIGURE 1 Representative electron micrographs of the P-face of the medium-exposed plasma membrane of Neuro-2A cells at three characteristic time points in the cell cycle: (*a*) mitosis (0 h); (*b*) early G_1-phase (1 h); (*c*) late S-phase (7 h). The magnification (252,000) is the same as that used for digitizing the coordinates of the IMP. Bar, 0.05 μm. Shadowing direction is indicated by arrow.

variation in IMP density is relatively large compared to that of cells from other phases in the cell cycle: mean ± SD (N) was 1,254 ± 439 IMP/μm^2 (11). Evidently, mitotic cells show extreme heterogeneities in local IMP density.

The total IMP density in replicas of E-faces fluctuates during the cell cycle partially in a different way. It remains relatively constant at ~700 IMP/μm^2 till 5–6 h after mitosis, but in the second half of the cell cycle the IMP density in E-faces is modulated qualitatively as similarly observed for P-faces, with a maximum of ~1,000 IMP/μm^2 at the end of S-phase (8 h).

IMP-Size Distribution and the Density of IMP-Subclasses

The observed modulation in the total IMP density during the cell cycle suggests that plasma membrane assembly is a cell-cycle-dependent process. An analysis of the IMP-size distribution can give information as to possible time-dependent insertion or rearrangement of particular IMP-forming molecular complexes. Taking the IMP diameter as a measure for the apparent IMP size, we determined the frequency distributions of IMP per 10 Å diameter class for each of the replicas. These distributions were pooled for each time point, and Fig. 3 presents the results for the P-faces at a number of characteristic time points, i.e. mitosis, early G_1-, late G_1-, and S-phase, in terms of absolute and relative frequency distributions. For these time points the IMP-size distributions are all significantly different, when compared by the Kolmogorov-Smirnov two sample test (22). Thus, not only does the total IMP density vary during the cell cycle, but also the apparent size distribution within the IMP population is subject to cycle-dependent variation. As can be seen from Fig. 3 the diameter of the IMP generally varies from 30 Å to 150 Å, but occasionally a few IMP with diameter up to 170 Å were found. Mitotic cells (t = 0 h) are characterized by relatively small IMP. Although the total IMP density does not change significantly in the very early G_1-phase (t = 0.5 h), a drastic shift from small to larger IMP is observed in this short period. During S-phase a gradual shift in the distribution towards smaller IMP sizes can be seen. Apparently, different IMP-size classes contribute in different periods in the cell cycle to the modulation in total IMP density, as described above.

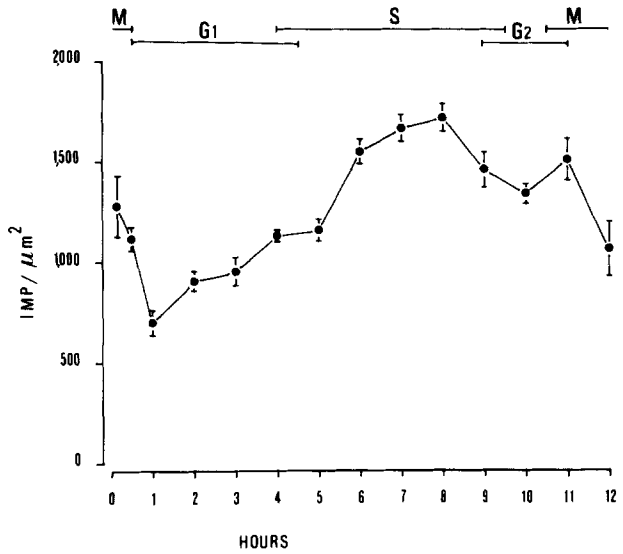

FIGURE 2 Total IMP-density (mean ± SEM) during the cell cycle of Neuro-2A cells. Usually, 10 electron micrographs, each representing 0.5 μm^2 membrane area, were analyzed for each time point, whereby a total number of 72,462 IMP were digitized. The diameters and relative coordinates of these IMP were used for the further analysis.

Fig. 4 illustrates in more detail the variations in the density of IMP-subclasses during the cell cycle. For practical reasons we have pooled the results so that histograms are given for four

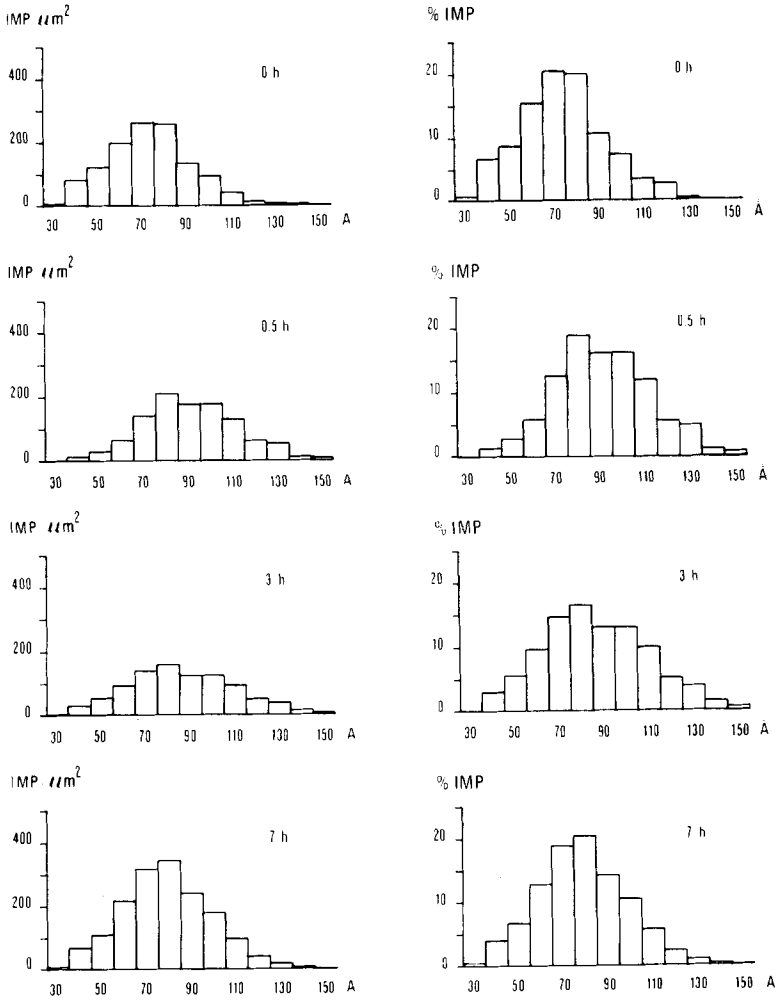

FIGURE 3 Histograms of the IMP-density as a function of the IMP-diameter (left column), and of the relative frequency distribution of the IMP-diameter (right column) at four characteristic time points in the cycle of Neuro-2A cells: mitosis (0 h), early G_1-phase (0.5 h), late G_1-phase (3 h), and late S-phase (7 h). The spatial resolution of the method was 10 Å.

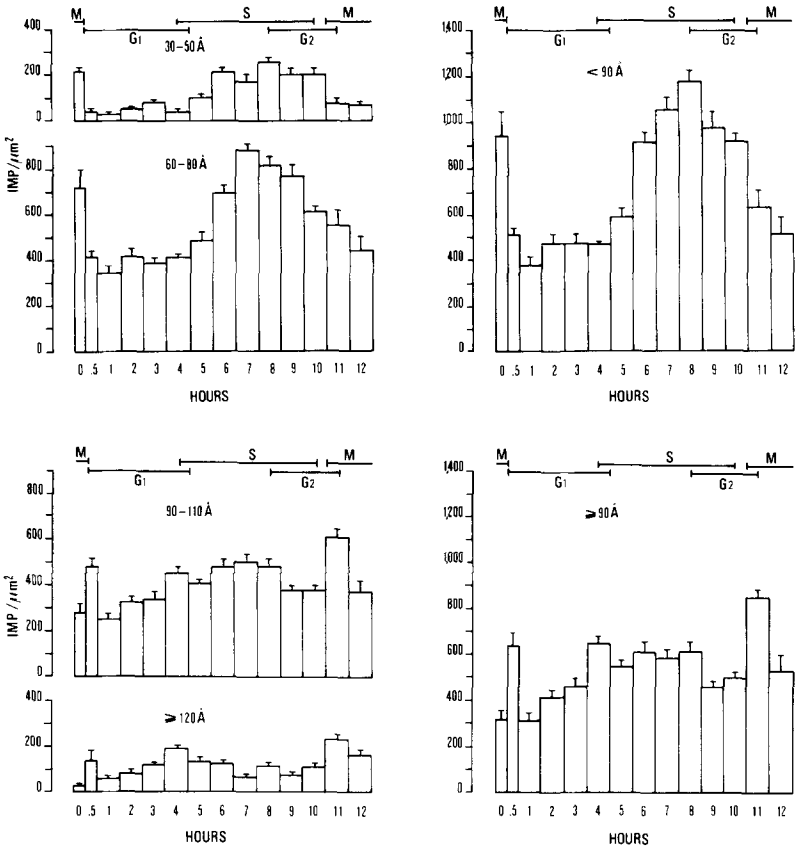

FIGURE 4 Density (mean ± SEM) of IMP-subclasses during the cell cycle of Neuro-2A cells. Left column: IMP-diameter ranges 30–50 Å, 60–80 Å, 90–110 Å and ≥120 Å, respectively. Right column: Pooled data for small IMP (<90 Å) and large IMP (≥90 Å), respectively.

subclasses with diameters of 30–50 Å, 60–80 Å, 90–110 Å and ≥120 Å, respectively. Qualitative comparison of the fluctuations in IMP density for these subclasses shows that two modulation patterns can be distinguished: the fluctuations in the density of IMP with diameters < 90 Å (small IMP) are different from those of IMP with diameter ≥ 90 Å (large IMP), but within each of both classes only minor qualitative differences are apparent. The densities pooled for small and large IMP are also given in Fig. 4. Small IMP are predominant in mitosis. Their density drops rapidly by 50% in the early G_1-phase (t = 0.5 h), remains constant during G_1-phase, doubles from the G_1/S transition till mid-S-phase, and decreases again through G_2-phase. Large IMP have a minimal density in mitosis. Their density doubles transiently in the early G_1-phase (0–1 h), doubles again gradually during further progression through G_1-phase, after which it remains approximately constant, except for a transient peak shortly before the next mitosis.

E-faces were analyzed similarly. As mentioned before, reproducibility of the analysis of E-faces was far from optimal. Taking this into account, we can nevertheless make some cautious conclusions. IMP in E-faces show a similar size range as found in P-faces (30–170 Å), with very few exceptionally large IMP with diameters up to 220 Å. Comparison of size distributions from different time points in the cell cycle did not yield indications for significant differences. This implies that our results do not indicate that shifts in the size distribution of IMP in P-faces are reflected in apparent changes in the IMP-size distributions of E-faces.

In conclusion, characteristic differences in IMP-density and IMP-size distribution in the P-face can be attributed to the various phases of the cell cycle. Furthermore, there is a clear difference between the modulations in density with time for small and large IMP, respectively, but within each of both IMP-classes the IMP are formed in a coordinated, time-dependent way.

Fractional IMP Area

If indeed IMP can be considered as structural manifestations of membrane (glyco)proteins, preferential insertion of membrane lipids in certain phases of the cell cycle might be detectable as a decrease in the relative surface area occupied by the IMP. Considering the IMP as spherical entities, we can calculate the relative area occupied by the IMP in the fracture plane of the membrane (Fig. 5). During the cell cycle this fraction varies between 5% and 10% of the total membrane area, without correction for IMP-free areas located in surface irregularities, such as are present in particular in mitotic cells.

During the greater part of the cell cycle, from early G_1- till late S-phase, the relative IMP-area increases gradually. From late S- till early G_1-phase a decrease is observed interrupted by two periods of transient increase at the onset (11 h) and end (0.5 h) of mitosis. Taking also into account the appearance and disappearance of IMP-free areas in this period, we interpret these changes as caused by preferential lipid insertion around mitosis, accompanied by transient rearrangements of membrane components during this period.

Lateral IMP Distribution

The lateral IMP-distribution in P-faces was analyzed for the total IMP-population (30–170 Å) and the following overlapping IMP-diameter classes: 30–90 Å, 50–110 Å, 70–130 Å, and

90–150 Å. The first and last subclasses correspond to the earlier distinguished small and large IMP. Two grid sizes were used for subdividing the electron micrographs: three and six times the maximum diameter of the selected IMP-range, respectively. A further increase of the grid size did not yield significant new information. The same replicas were analyzed for their lateral IMP-distribution as used for determining the IMP-density and IMP-size distribution. The frequency distributions of the number of subareas as a function of the number of IMP per subarea were pooled for the different replicas of a given time point. The Poisson variance test was applied to this multiple of 0.5 μm^2 membrane area. For discrimination between random, aggregated, and dispersed distributions, a 1% significance level is used throughout the text.

The lateral IMP-distribution appeared to be strongly modulated during the cell cycle, indicating the existence of stage-specific constraints on the lateral mobility of IMP-forming molecules. Considering the total IMP population (Fig. 6), mitotic cells show a significant IMP-aggregation at both grid sizes, though extremely pronounced at the larger grid size, indicating a significant micro- and macroscopic grouping of IMP. As the cells proceed into the early G_1-phase, and reattach more firmly to the substratum, a rapid rearrangement of the IMP takes place. IMP acquire a random distribution at both grid sizes, as if directional constraints are released. From late G_1- till G_2-phase the IMP distribution depends on the grid size. Macroscopic, nonrandom heterogeneities in their distribution remain absent, as shown by their random distribution at the large grid size, but new constraints lead to a dispersed distribution at the small grid size.

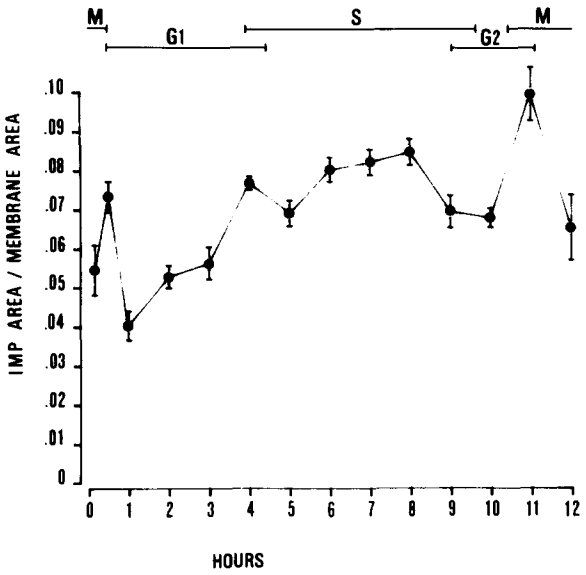

FIGURE 5 The fractional surface area occupied by IMP in the plane of the membrane during the cell cycle of Neuro-2A cells. The surface area was determined from the IMP-size distribution, taking the IMP as spherical structures.

The lateral distribution of the IMP subclasses is similar to that of the total IMP population, with only a few exceptions (Fig. 7). All subclasses show a random distribution at small grid size in mitosis, in contrast with the aggregated state of the total IMP population. Apparently, this aggregation is due to grouping of IMP of different sizes. During further progression of the cell cycle, only the large IMP (90–150 Å) behave to some extent differently from the rest. They show a random distribution at small grid size except for two periods of dispersion: the G_1/S transition and G_2-phase. At large grid size this is the only IMP subpopulation that remains aggregated from mitosis through most of the G_1-phase, as if the postmitotic IMP-rearrangement is delayed for large IMP.

DISCUSSION

In the present study we have used freeze-fracture electron microscopy to detect modulations in the internal structure of the plasma membrane during the cell cycle of Neuro-2A cells. A computer-assisted method (15) was applied to describe these modulations quantitatively in terms of the density, size distribution, and lateral distribution of the observed IMP. The differential density distribution analysis at variable grid size (15) proved to be a powerful method for detecting subtle alterations in the lateral IMP-distribution. By this method, properties of the dynamic organization of the plasma membrane can be detected that otherwise would remain obscured. The results demonstrate that the plasma membrane is changing its structural features continuously during the life history of a cell. They provide evidence for a cell-cycle-dependent insertion and dynamic reorganization of membrane components, such

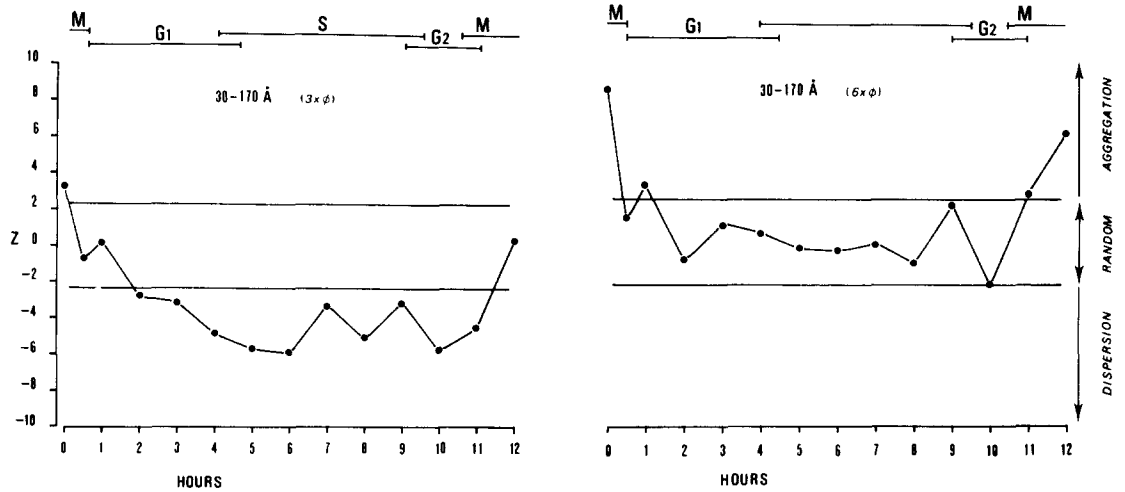

FIGURE 6 Lateral distribution of the total IMP-population at grid sizes of three (left panel) and six (right panel) times the maximum IMP-diameter, respectively, during the cell cycle of Neuro-2A cells. The horizontal lines indicate the 1% significance levels for the approximate normal deviate Z, as given by the Poisson variance test.

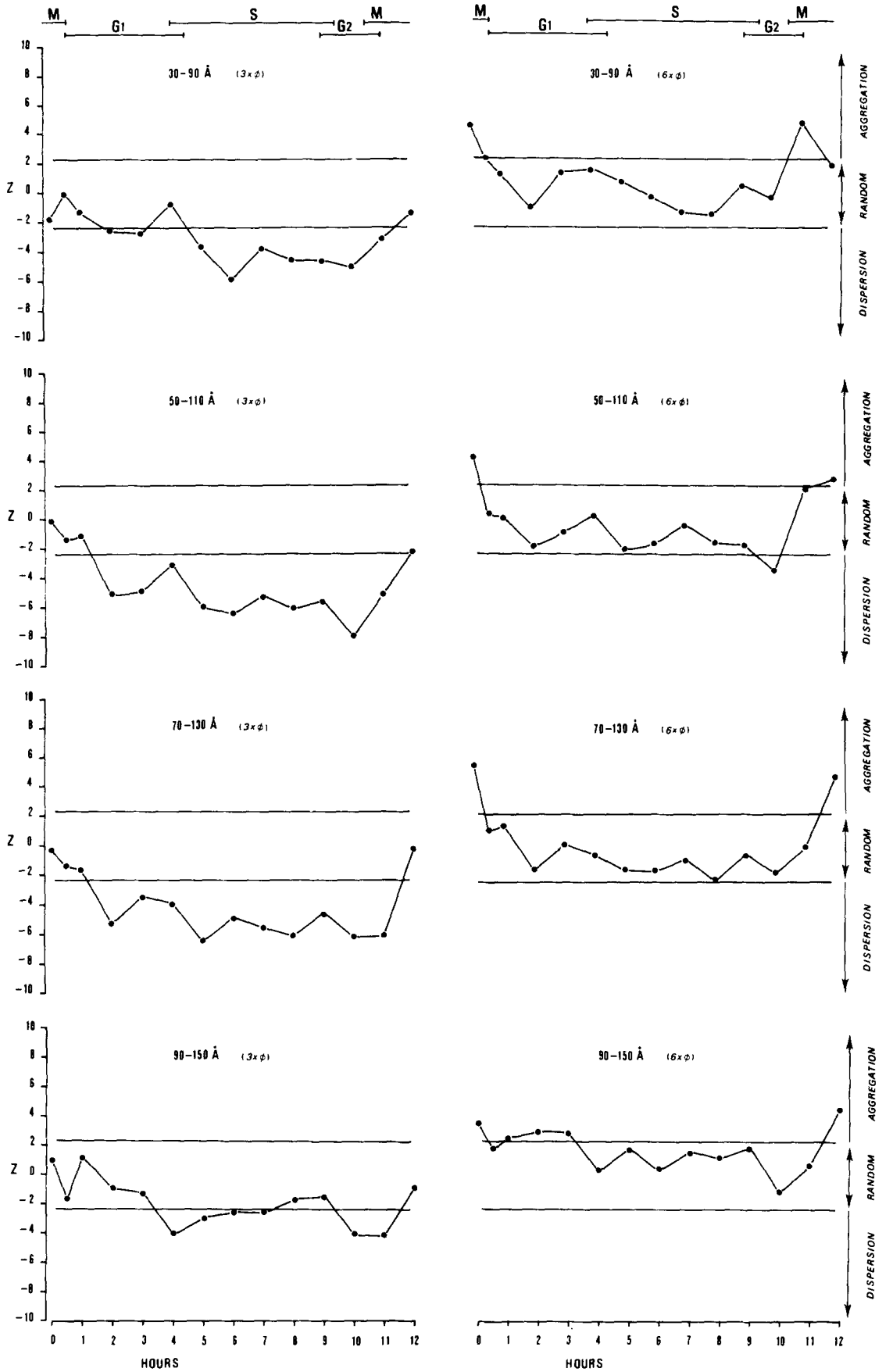

FIGURE 7 Lateral distribution of four overlapping IMP-subpopulations during the cell cycle of Neuro-2A cells. The IMP-subpopulations have diameters ranging from 30 to 90 Å, 50 to 110 Å, 70 to 130 Å, and 90 to 150 Å, respectively. The distributions were analyzed at grid sizes of three (left column) and six (right column) times the maximum of the selected diameter range. The horizontal lines indicate the 1% significance levels for the approximate normal deviate Z, as given by the Poisson variance test.

that characteristic structural and dynamic properties can be attributed to the various cell cycle phases.

Based on the assumption that the IMP represent (glyco)protein complexes embedded in the membrane lipid matrix (23), the IMP-density and -size-distribution provide information as to alterations in plasma membrane composition. For a proper interpretation of these data, it should be realized that membrane growth during the cell cycle is not linear with respect to time. The cell surface area of Neuro-2A cells, determined from their diameter after maximum hypotonic swelling, remains constant at ~1,000 μm^2/cell from mitosis until the G_1/S transition, after which it gradually increases to 1,350 μm^2/cell at mid-S-phase. No further increase takes place till late G_2-phase, but before or in mitosis the cell surface area suddenly increases again and roughly doubles as compared with early G_1 cells (4). Most likely, the net cell surface area is predominantly determined by the membrane lipids, and thus net lipid insertion into the plasma membrane seems to be restricted to S-phase and, more pronounced so, to a short period around mitosis.

Although alternative explanations could be given, we consider the decrease in IMP density around mitosis as an indication for rapid preferential lipid over protein insertion into the plasma membrane during this phase. Support for this view comes from the observed surface activity in phase-contrast time-lapse cinematography and from the appearance of numerous surface protrusions as visualized in scanning electron micrographs of Neuro-2A cells (our own unpublished observations), as well as in other cells (20) in this period of net cell surface growth. These surface irregularities appear, after freeze-fracturing, as IMP-free areas and could provide a large storage of segregated, newly incorporated membrane lipids (1). Concomitant with these compositional changes the dynamic organization of the plasma membrane is radically changed. The rotational and lateral mobility of membrane lipids transiently drops to a low level (13, 14) and also the lateral diffusion of membrane proteins reaches a minimum during mitosis (13). Correspondingly, the aggregated lateral IMP-distribution at both grid sizes indicates the presence of constraints on the lateral mobility of the represented molecules in mitotic cells, which is supported by the reported distribution of specific surface receptors in mitosis (8). In a separate study we have studied the structural features of the mitotic cell and the structural reflections of membrane growth in more detail. Also, in nonfixed mitotic cells, directly frozen by propane jet-freezing, the plasma membrane shows similar gross heterogeneities in IMP distribution, as described here (to be published elsewhere).

In the early G_1-phase a radical reorganization of membrane components within the plane of the membrane takes place, which coincides with (or leads to) the flattening and reattachment of the rounded mitotic cells. While the total surface area remains constant, the protrusions gradually disappear during a process of surface stretching. Within 30 min after mitosis the density of small IMP (<90 Å) is reduced by a factor of two, while the density of large IMP (≥90 Å) doubles. Even more pronounced are the changes in density for the smallest (30–50 Å) and largest (≥120 Å) IMP, which show a reduction and increase, respectively, by a factor of five. At the same time the IMP, under all conditions tested, shift towards a random lateral distribution, which we interpret as a loss of constraints on their lateral mobility. Support for this view comes from the earlier observed sudden increase in the lateral mobility of membrane lipids and proteins (13) and in membrane-fluidity (14) during this period. In view of these changes in membrane fluidity the possibility should be considered that the changes in IMP-size distribution around mitosis are partially or fully due to the displacement of integral membrane proteins perpendicular to the fracture plane (5). So far, we have no direct evidence for this hypothesis, but future experiments should verify this interesting possibility. Similarly, the possibility should be considered that larger complexes are formed through the aggregation of smaller ones. Furthermore, it could be argued that the changes in IMP density result from rearrangements of IMP between the medium-exposed and substratum-attached regions of the plasma membrane, as the cells reattach more firmly. Preliminary analysis of the P-face of the substratum-attached membrane showed, however, that the IMP density at both sides of the cells changes rather independently during the cell cycle, the density being constant at the attached site from mitosis till early S-phase. All together, our data indicate that in early G_1-phase the various membrane components become more mobile and start to intermingle so that macroscopic heterogeneities within the plane of the membrane disappear. It could well be that the increased fluidity of the plasma membrane creates conditions that facilitate the integration of membrane proteins (9).

Further progression of the cells through the G_1-phase is marked in particular by: (*a*) an exclusive increase in the density of large IMP, suggesting the insertion of specific classes of membrane proteins, and (*b*) a gradual change in the lateral IMP distribution at the small grid size to a dispersed distribution, as if new constraints on IMP mobility appear. This coincides with a gradual decrease in the lateral mobility of membrane proteins, while membrane lipids remain in a relatively mobile state (13). A plausible explanation for these phenomena is the formation of an anchorage of membrane components to cytoskeleton elements (7).

As mentioned above, a 35% increase in cell surface area takes place during S-phase (4). In contrast to G_1-phase, now the small IMP increase exclusively in density, which indicates a preferential insertion of small IMP-forming components. Compensating for changes in cell surface area reveals that the number of small IMP per cell is constant at $\sim 4 \times 10^5$ IMP per cell during G_1-phase, rapidly increases during the early S-phase (4–7 h) to $\sim 14 \times 10^5$ IMP per cell, and then remains approximately constant till G_2-phase. In contrast, the number of large IMP per cell increases almost linearly with time from early G_1-phase (3×10^5 IMP per cell) till mid-S-phase (8×10^5 IMP per cell), with no further substantial changes till G_2-phase.

During S-phase all the IMP subpopulations show a dispersed lateral distribution at the smaller grid sizes, as if some anchorage persistently restricts their mobility within the plane of the membrane. A further decrease in protein mobility at constant lipid mobility in this period was reported before (13), and is in agreement with this explanation. At the larger grid sizes the absence of macroscopic spatial heterogeneities is demonstrated by the random distribution of all IMP subpopulations.

Necessarily, cells tend to desynchronize with time and this affects the accuracy of the time resolution in the late cell cycle events in a negative way. Nevertheless, it is clear that the plasma membrane is reorganized radically and rapidly as cells prepare themselves for the next mitosis and cell division (G_2-, M-phase). The cell surface area increases from 1.4 to more than two times that of the early G_1-phase (4), which would require a rapid insertion of membrane lipids, possibly reflected

in the formation of IMP-free areas in the mitotic cell. During this process the density of the small IMP decreases by a factor of two, whereas the large IMP shows a transient increase of 1.7 times. At the small grid size the IMP lose their dispersed distribution and become random again. At the large mesh size, all IMP subpopulations become aggregated but the small IMP show the more pronounced aggregation. It seems plausible, therefore, that the period just before mitosis is dominated by a rapid lipid insertion into the plasma membrane, and a loss of anchorage of membrane proteins to the cytoskeleton. These events coincide with a rapid decrease in membrane lipid mobility and fluidity, while protein mobility becomes minimal (13, 14). Whether lipid insertion in itself is a driving force for macroscopic IMP aggregation remains to be established.

At present we can only compare our data on the modulations in total IMP density during the cell cycle with those obtained by others (10, 21, 25), because data on other features of the internal membrane structure are not available. Qualitatively, Scott et al. (21) described similar fluctuations in IMP density during the cell cycle of L cells and Chinese hamster cells. However, also the absence of such fluctuations was reported for other cell types (10, 25). The reasons for this discrepancy are yet unclear.

In conclusion, we have shown that Neuro-2A cells modify their plasma membrane continuously while progressing through the cell cycle. Each of the cell cycle phases appears to be characterized by specific structural membrane changes that can be interpreted in terms of the incorporation of particular membrane components and dynamic reorganizations within the plasma membrane. It might be expected that the observed structural changes will be reflected in modulations of functional properties of the plasma membrane. Recent studies from our laboratory on the active and passive cation transport properties and the electrical membrane properties during the cell cycle of the same cell type (4, 11, 12, 16, 17) provide strong support for this view. Specific alterations in these membrane properties coincide with specific structural changes. As membrane transport functions, membrane-bound enzymes, and receptor sites control to a large extent the intracellular milieu and the interaction of the cell with its external environment, it seems likely that the described intrinsic membrane modulations are a structural manifestation of alterations in membrane functions involved in the regulation of the cell cycle.

We thank Dr. E. J. J. van Zoelen for his valuable comments, and Ms. E. C. Ekelaar for preparing the manuscript.

Received for publication 14 July 1981, and in revised form 31 August 1982.

REFERENCES

1. Bluemink, J. G., and S. W. de Laat. 1977. Plasma membrane assembly as related to cell division. *Cell Surf. Rev.* 4:403–461.
2. Bluemink, J. G., and L. G. J. Tertoolen. 1978. Freeze-fracture electron microscopy of the plasma membrane of the Xenopus egg: evidence for particle-associated filaments. *Cytobiologie.* 16:358–366.
3. Bluemink, J. G., L. G. J. Tertoolen, P. H. J. Th. Ververgaert, and A. Verkley. 1976. Freeze-fracture electron microscopy of preexisting and nascent cell membrane in cleaving eggs of Xenopus laevis. *Biochim. Biophys. Acta.* 443:143–155.
4. Boonstra, J., C. L. Mummery, L. G. J. Tertoolen, P. T. van der Saag, and S. W. de Laat. 1981. Cation transport and growth regulation in neuroblastoma cells. Modulations of K^+ transport and electrical membrane properties during the cell cycle. *J. Cell. Physiol.* 107:75–83.
5. Borochov, H., and M. Shinitzky. 1976. Vertical displacement of membrane proteins mediated by changes in microviscosity. *Proc. Natl. Acad. Sci. USA.* 73:4526–4530.
6. Branton, D. 1966. Fracture faces of frozen membranes. *Proc. Natl. Acad. Sci. USA.* 55:1048–1056.
7. Edelman, G. M. 1976. Surface modulation in cell recognition and cell growth. *Science (Wash. DC).* 192:218–226.
8. Garrido, J. 1975. Ultrastructural labelling of cell surface lectin receptors during the cell cycle. *Exp. Cell Res.* 94:159–175.
9. Ito, K., T. Sato, and T. Yura. 1977. Synthesis and assembly of the membrane proteins in E. coli. *Cell.* 11:551–559.
10. Knutton, S. 1976. Structural changes in the plasma membrane of synchronized P815Y mastocytoma cells. *Exp. Cell Res.* 102:109–116.
11. de Laat, S. W., and P. T. van der Saag. 1982. Modulation of structure and function of the plasma membrane in the cell cycle of neuroblastoma cells. *In* Genetic Expression in the Cell Cycle. Vol. II. G. M. Padilla and K. S. McCarthy, Sr., eds. Academic Press, New York. 337–361.
12. de Laat, S. W., and P. T. van der Saag. 1982. The plasma membrane as a control site in growth and differentiation of neuroblastoma cells. *Int. Rev. Cytol.* 74:1–54.
13. de Laat, S. W., P. T. van der Saag, E. L. Elson, and J. Schlessinger. 1980. Lateral diffusion of membrane lipids and proteins during the cell cycle of neuroblastoma cells. *Proc. Natl. Acad. Sci. USA.* 77:1526–1528.
14. de Laat, S. W., van der Saag, P. T., and Shinitzky, M. 1977. Microviscosity modulation during the cell cycle of neuroblastoma cells. *Proc. Natl. Acad. Sci. USA.* 74:4458–4461.
15. de Laat, S. W., L. G. J. Tertoolen, and J. G. Bluemink. 1981. Quantitative analysis of the numerical and lateral distribution of intramembrane particles in freeze-fractured biological membranes. *Eur. J. Cell Biol.* 23:273–279.
16. Mummery, C. L., J. Boonstra, P. T. van der Saag, and S. W. de Laat. 1981. Modulation of functional and optimal (Na^+-K^+)ATPase activity during the cell cycle of neuroblastoma cells. *J. Cell. Physiol.* 107:1–9.
17. Mummery, C. L., J. Boonstra, P. T. van der Saag, and S. W. de Laat. 1982. Modulations of Na^+ transport during the cell cycle of neuroblastoma cells. *J. Cell. Physiol.* 112:27–34.
18. Nicolson, G. L. 1976. Transmembrane control of the receptors on normal and tumor cells. I. Cytoplasmic influence over cell surface components. *Biochim. Biophys. Acta.* 457:57–108.
19. Nicolson, G. L. 1976. Transmembrane control of the receptors on normal and tumor cells. II. Surface changes associated with transformation and malignancy. *Biochim. Biophys. Acta.* 458:1–72.
20. Porter, K., D. Prescott, and J. Frye. 1973. Changes in surface morphology of Chinese Hamster ovary cells during the cell cycle. *J. Cell Biol.* 57:815–836.
21. Scott, R. E., R. L. Carter, and W. R. Kidwell. 1971. Structural changes in membranes of synchronized cells demonstrated by freeze-cleavage. *Nature New Biol.* 233:219–220.
22. Siegel, S. 1956. Nonparametric statistics for the behavioral sciences. McGraw-Hill Book Comp., Inc., Tokyo.
23. Singer, S. J., and G. L. Nicolson. 1972. The fluid mosaic model of the structure of cell membranes. *Science (Wash. DC).* 175:720–731.
24. Snedecor, G. W., and W. G. Cochran. 1967. Statistical methods. The Iowa State University Press, Ames, IA.
25. Torpier, G., L. Montagnier, J. M. Biguard, and P. Vigier. 1975. A structural change of the plasma membrane induced by oncogenic viruses: quantitative studies with the freeze-fracture technique. *Proc. Natl. Acad. Sci. USA.* 72:1695–1698.
26. van Zoelen, E. J. J., P. T. van der Saag, and S. W. de Laat. 1981. Family tree analysis of a transformed cell line and the transition probability model for the cell cycle. *Exp. Cell Res.* 131:395–406.